Journal of Materials Chemistry A

Accepted Manuscript

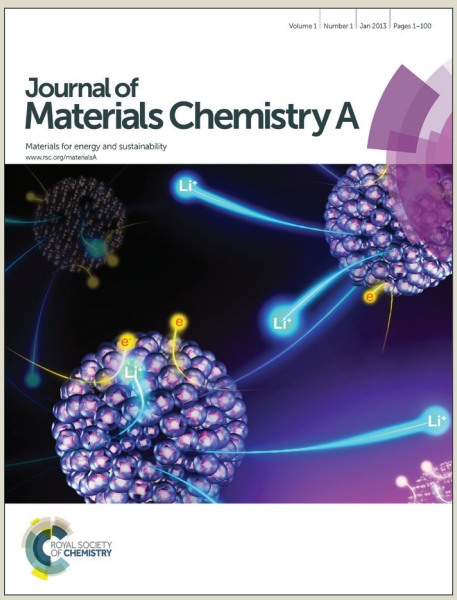

ROYAL SOCIETY OF CHEMISTRY

www.rsc.org/materialsA

Journal Name RSC Publishing

COMMUNICATION

Stepwise interfacial assemblied nickel-cobalt-hydroxide hetero-accumulated nanocrystalline walls on reduced graphene oxide/nickel foams: an adjustable interface design for capacitive charge storage

Cite this: DOI: 10.1039/x0xx00000x

Received 00th January 2012,
Accepted 00th January 2012

DOI: 10.1039/x0xx00000x

www.rsc.org/

Zhongyu Qian,[a] Tao Peng,[a] Liangti Qu,[b] Jun Wang[a,*] and Peng Wang [c,*]

To achieve a balance of a high specific capacitance between the electroactive materials and electrodes with adjustable specific energy and power, evaporation-induced nickel-cobalt-hydroxide hetero-accumulated nanocrystalline walls on reduced graphene oxide/nickel foams are presented by different Ni-doping and dipping numbers. The flexible solution-based strategy promotes a new interface design for capacitive charge storage.

Recent research and development has focused on the design of advanced capacitive charge storage devices, and the high-efficiency electrochemical energy storage requires an excellent interface between the electronic-transporting phase (electrode) and the ionic-transporting phase (electrolyte).[1-3] Nanotechnology has been intensively investigated for the development with high power and energy densities.[4-6] A range of nanomaterials, such as carbon-based electric double-layer capacitive (EDLC, such as graphene-based materials) materials, pseudocapacitive transition-metal-based oxides or hydroxides (TMOs, such as $Co(OH)_2$, $Ni(OH)_2$), has gained prominence with high specific surface area and small dimensions.[7-9] Most traditional research focused on active materials and synthesis, as it has been widely accepted that the interface of electrode materials plays a key role, considerable attentions have been paid on the interface and entire electrode system to solve all kinds of technological challenges.[10-12]

Building heterostructured nanowire arrays on conductive substrates provides a robust adhesion for the electrode system with a few successful strategies (such as electrodeposition, hydrothermal synthesis).[13-15] The interval space formed between neighboring makes easy diffusion of ionic-transporting region, and core nanowires could act as backbones to guide the shell materials preferentially deposited with enhanced electrochemical properties.[16-18] However, it's better to say that the fabrication has successed in specific capacitance for electroactive material rather than for electrodes. A small electroactive mass loading could be hardly used for practical applications. Moreover, cost-effective and simple methods are still needed for scale-up. A key challenge for the fabrication of heterostructured nanoarchitectures built on conductive substrates is to build up an integrated architecture step by step and utilize the better interface of the substrates, in which the electrode/electrolyte interface guarantees a fast ion and electron transfer, meanwhile, the optimal physical space can be manifested with a large mass loading.

In the sight of the crystal growth mechanism in building heterostructured nanowire arrays, 'self-assembly' and 'oriented attachment' describes the spontaneous self-organization and joining of adjacent particles at the interface.[19,20] It occurs coinstantaneously to provide a robust adhesion and optimal physical space together, which leads to a limited mass loading. Therefore, if the process could be done separately, the fabrication would be more flexible and controllable. Based on these, the nano-architecture process could be achieved in two steps: the formation of nanoscale building blocks and the interfacial assembly with substrates.[21,22] As a proof-of-concept, we present a flexible solution-based strategy as illustrated in Fig. 1A. First, three-dimensional porous nickel foams with reduced graphene oxide (rGO) coating were prepared by a simple "dip and dry" process. Next, nickel-cobalt-hydroxide (NCH) nanoscale building blocks could be synthesized by a mild mixing of NaOH ethanol solution and $NiCl_2$-$CoCl_2$ aqueous solution. Here, the rGO/nickel foams (rGO/NF) were used as substrates for "adhering", and solvent-evaporation-induced "interfacial assembly" to coerce NCH nanoscale building blocks on the rGO/NF. Consequently, with different nickel-doping and dipping numbers, the NCH/rGO/NF exhibit a balance of high specific capacitances between the electroactive materials and the electrodes with adjustable specific energy and power. The interfacial assembly process could be repeated easily and conveniently, which promotes an optimal electrode/electrolyte interface with a large mass loading for potential applications in lithium-ion batteries, electrochemical or photocatalysis, and energy conversion storage.

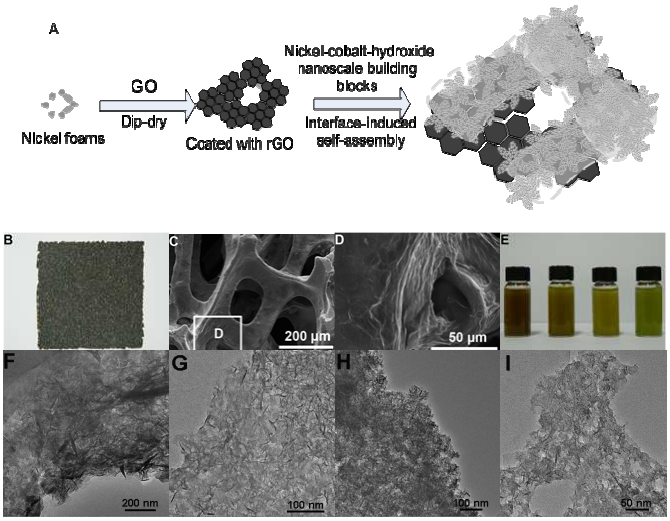

Fig. 1 Morphologies of the rGO/nickel foam and NCH nanoscale buliding blocks. (A) Schematic illustration of the nanoarchitecture on the rGO/NF from NCH nanoscale building blocks. (B) Photographs of the nickel foams with rGO coatings. (C-D) SEM images of the rGO/NF. (E) Photographs of the NCH suspensions prepared. (F-M)TEM images of the suspensions with different Ni-content in a molar fraction. (F:0; J:0.33;H: 0.5; I: 0.67)

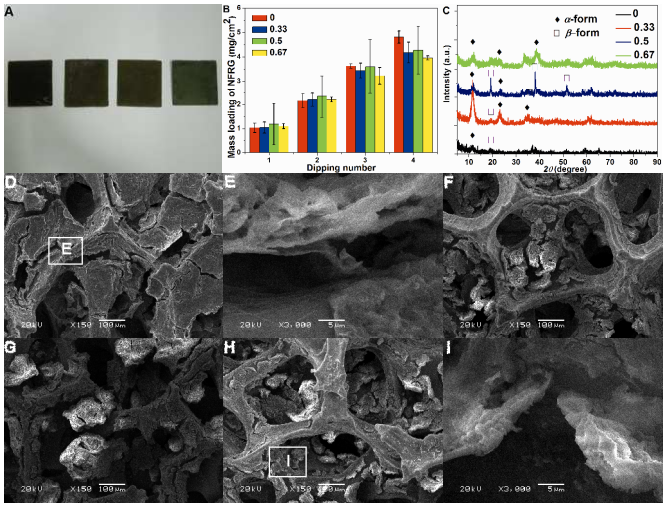

Fig. 2 Some characterizations of the rGO/NF with self-assemblied NCH hetero-accumulated nanocrystalline walls. (A) Photographs of the nickel foams with rGO coatings. (B) Mass loading of the rGO/nickel foam versus dipping number with different Ni-content in molar fraction. (C) XRD of the NCH powders scratched from the NCH/rGO/NF. (D-I) SEM images of the NCH/rGO/NF with different Ni-content in a molar fraction. (D,E:0; F:0.33; G: 0.5; H,I: 0.67).

Alignments of nanocrystalline phases with different morphologies and microstructures show substantial differences in electrochemical performances.[23] Interfacial designs for electron and ion transfer are affected by chemical and physical properties of substrates, which implies the importance surface modification and functionalization.[24-26] Inspired by the phenomenon that the functional groups of textiles promote the solvent-evaporation-induced 'interfacial assembly' with solutes,[27] three-dimensional porous nickel foams with rGO coating were prepared by a simple "dip and dry" process. Graphene oxide could provide a weak acid environment (pH: 5.00) to transform etched nickel to nickel hydroxides,[28] which guarantee robust adhesion with the nickel foams (Fig. 1.B). Scanning electron microscopy (SEM) images (Fig. 1C,D) clearly show the nickel foams are covered with folded rGO coatings, and the rGO coating may stretch out along the nickel foams. X-ray diffraction (XRD) indicates the reduction of GO after the "dip and dry" process , while, Fourier transform infrared (FTIR) analysis confirms the retention of the functional groups of rGO (Fig. S1).[29] The interactions of these functional groups with suitable nanoscale building blocks will provide an enhanced bonding.

To successfully fabricate nanoarchitectures built on conductive substrates, suitable nanoscale building blocks need to be prepared. The process could be achieved by dropping NaOH ethanol solution into $NiCl_2$-$CoCl_2$ aqueous solution slowly with colloidal hydroxides produced (Fig. 1E). As the samples preparation for transmission electron microscopy (TEM) is similar to the interface-induced assembly of the suspensions on substrates, the TEM tests supply more information about the nanoscale building blocks for interfacial assembly than the materials themselves (Fig. 1F-I). Irregular clusters or piles cluttered with minute nanocomponents prove that the fusion of the nanoscale building blocks leading to bulk single-crystalline structures could be inhibited.[20] Ions are generally considered to adsorb at edges and kink of the developing crystal surface stopping it from further growth, while mesoscale self-assemblied hetero-accumulated nanocrystalline walls could be transformed from the nanocale building blocks. These properties make the formation of nanoscale building blocks and the interfacial assembly with substrates step by step possible, and the physical space of mutual three-dimensional translational order of various NCH nanocrystals will be kinetically facile for peseudocapacitive effects.[30,31]

Ions adsorbed at edges benefit the well dispersion of nanoscale building blocks, while they promote 'hit and stick' behavior that forms fractal nanoparticle networks in the solvent-evaporation-induced interifacial assembly together with diffusion-limited cluster aggregation.[32] The interfacial assembly on the rGO/NF (Fig. 2.A) replaces the liquid with gas, when the electrodes are immersed in an electrolyte, it interpenetrates solid-state with liquid-state, that is to say, it interpenetrates efficient ion and electron transport. The variation of the mass loading on the rGO/NF with the dipping number is nearly equal, but the material at 0.5 is fluctuating (Fig. 2B). XRD shows higher degrees of crystallinity for the NCH at 0.33 and 0.5 (Ni-content in a molar fraction), compared with the NCH at 0 and 0.67, which is in accordance with the differences in the cross-link of the NCH nanocrystals (Fig. 1J-M). The hydrotalcite-like phase (α-form, JCPDS:46-0605) and the brucite-like phase (β-form, JCPDS:45-0031) are observed for the NCH,[33,34] the fluctuating NCH at 0.5 in Fig. 2B implies that the β-form may be not suitable for the interface assembly. SEM images show the characteristic of the interface between the NCH and the rGO/NF (Fig. 2D-K). For cobalt hydroxide, the aggregated films stand by the skeletons of the rGO/NF and cover the pores with cracks (Fig. 2D), and stacks of folded films could not be distinguished (Fig. 2H). As the Ni content increases, the films transform loose scatters of scales. It seems that the self-assemblied hetero-accumulated nanocrystalline walls were disordered on the rGO/NF. However, the physical space from reciprocal three-dimensional translational order of various NCH nanocrystals may benefit the electrodes with a large mass loading.

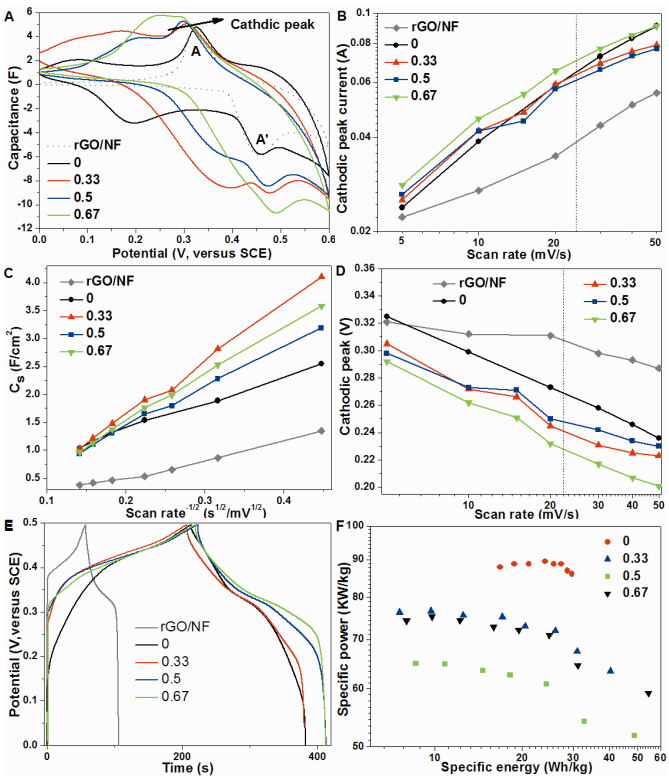

Fig. 3 Electrochemical characterizations of the NCH/rGO/NF with different Ni-content in a molar fraction. (A) Cyclic volammograms for different Ni-content in molar fraction at a scan rate of 5 mV s^{-1}. (B) *b*-value determination of the peak cathodic currents from 5 to 50 mV s^{-1}. (C) Specific capacitance (F cm^{-2}) versus $v^{-1/2}$. (D) The variation of the cathodic peak potential with the scan rate.(E) Charge and discharge curves at a current density of 6 mA cm^{-2}. (F) Ragone plots in a mass unit of the active materials (NCH).

To explore the electrochemical performances of the NCH with different Ni-contents, cyclic voltammetry (CV) was tested by a three-electrode system (Fig. 3A). A typical redox couple characteristic of Ni^{2+}-Ni^{3+} (A-A') is observed in the CV curve,[18] which serves as a marker for the NCH/rGO/NF. The peak current obeys an assumed relationship with the scan rate as follow:[35]

$$I = av^b \quad (1)$$

Where I is the peak current, v is the scan rate, a and b are the adjustable values. With the adjustable values, surface-controlled (b = 1) and diffusion-controlled (b = 0.5) could be separated (Fig. 3B). For the scan rates ranging from 5 to 20 mVs^{-1}, the b-values for the cathodic peak currents are ranging from 0.5 to 1 (Fig. S3A), pesudocapacitve contribution could be distinguished.[36] As the scan rates increase (> 20 mV s^{-1}), b-values decrease (< 0.5), the ohmic contribution and diffusion constrants/limitations become obvious.[37] The relationship between specific capacitance (C_s) and scan rate (v) shows the capacitance retention for different Ni-content (Fig. S3B). In a pot of Cs versus $v^{-1/2}$ (Fig. 3C), the slopes reveal that cobalt hydroxide has a better capacitance retention, Ni-doping could increase the capacitance at the cost of a poor retention. With the positions of the cathodic peak shifts increase from 5 to 50 mV s^{-1}, the suggest cobalt hydroxide has a relatively low resistance of the electrodes for the good contact between the electroactive materials and the conductive substrate, while, Ni doping obviously increases the resistance. (Fig. 3D).

The electrodes are also evaluated by the charging/discharging measurement at 6 mA cm^{-2}, as shown in Fig. 3E, Ni doping has a higher voltage plateaus than cobalt-hydroxide. For electrochemical energy storage, the plot of power against energy density (the Ragone plot) is calculated based on the charging/discharging curves at different current densities, as shown in Fig. 3F. To indicate the performances of the NCH better, the specific energy and specific power are based on the mass of the NCH. The cobalt hydroxide is distributed more densely in the specific energy at different current densities, and has a higher specific power than Ni-doping. The electrochemical performance could be derived from the following features for the NCH with different Ni-content. Firstly, for cobalt hydroxide, the aggregated films stand by the skeletons of the rGO/NF ensure good mechanical adhesion and facilitate transport of the electrolyte. Furthermore, the physical space of reciprocal three-dimensional translational order of various nanocrystals will be kinetically facile for peseudocapacitive effects. In addition, the films transform loose scatters of scales with Ni-doping, which obviously increases the resistance. The interface and charge-transfer resistance could be also calculated by electrochemical impedance spectra (EIS) as evidence (Fig. S4A-C). Besides, Ni-doping makes a faradaic contribution from battery-like diffusion-controlled with charge-transfer resistance, which leads to a higher capacitance at a small current, but a lower capacitance at a large current.

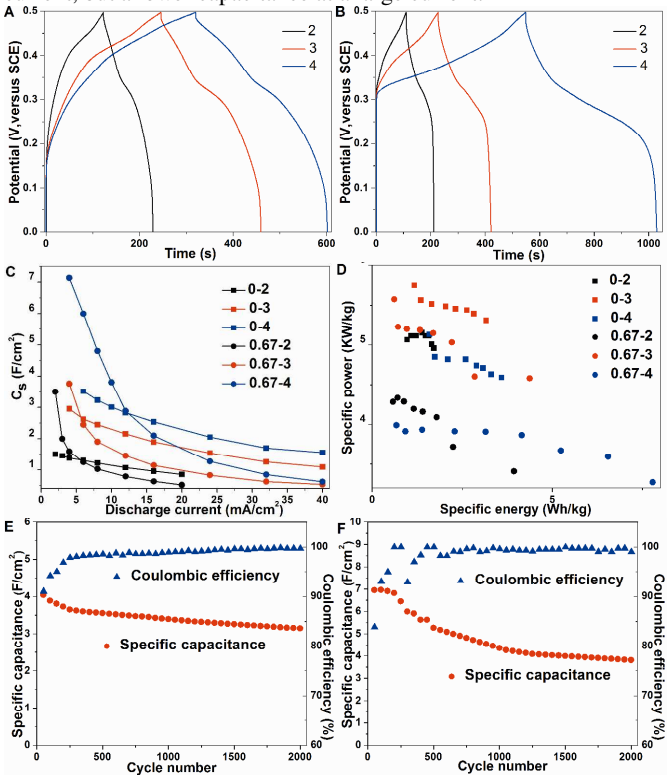

Fig. 4 Electrochemical characterizations of the NCH/rGO/NF with different dipping numbers. Charge and discharge curves for different Ni-content in a molar fraction (a: 0; b: 0.67) at a current density of 6 mA cm^{-2}. (C) Specific capacitance (F cm^{-2}) versus current density (mA cm^{-2}). (D) Ragone plots in a mass unit of the electrodes. Cycling performances of the electrodes with different Ni-content in a molar fraction (E:0; F:0.67) at a current density of 5 mA cm^{-2} for 2000 cycles.

To achieve a balance between the specific capacitance and capacitance, the electrochemical performances of the NCH/rGO/NF with different dipping numbers are significant. As the mass loading of the NCH increases, the capacitance increases with the shapes of the charging/discharging curves maintained with different dipping numbers (Fig. 4.A,B). Calculation of specific capacitance based on the area of the electrodes shows the mass effects of the active materials, The areal capacitance for Ni-doping could reach as high as 7.14 F cm^{-2}, but it fall behind the cobalt-hydroxide with a large current (>12 mA cm^{-2}), the areal capacitance for the cobalt-hydroxide are from 3.51 to 1.56 F cm^{-2} with less dependence with the current (Fig. 4.C). The specific energy and power has a maximum with the dipping numbers (the mass loading of the active materials). The cobalt-hydroxide benefits a high specific power and Ni-doping benefits a high specific energy (Fig. 4D). The cycling stability of the NCH/rGO/NF is also evaluated at 5 mA cm^{-2}, as shown in Fig. 4E and Fig. 4F. The high power cobalt hydroxide has a better capacitance retention (78.0% after 2000 cycling) than the Ni-doping (54.9%). Ni-doping increases the electroactive regions from the surface to the bulk, but there often exist volume change and crystallinity decrease in the charging/discharging. The irreversible transition leads to a poor electron transporting in the self-assemblied NCH hetero-accumulated nanocrystalline walls, and exhibits a poor capacitance retention.

Finally, in order to get a more clear impression about our results, we have included the tabulated information in Table 1. Slurry-pasting has obvious drawbacks including poor electron transport, but it is much more simple and cost-effective with a small mass loading, compared with a hydrothermal process.[13] However, a random distribution and extra weight of additives is undesirable for high performance. Layer-by-layer assembly could prepare nanoscale ordered layered nanocomposites, but is may be time-consuming and difficult for bulk-materials synthesis.[38] Compared with the table, our cycle retention is a little poor, but the specific capacitance is still higher than a traditional research after the cycling. Our strategy is aimed to process from a simple and cost-effective way to a fabrication with tunable space. It will be a powerful strategy to replace a hydrothermal or other heavy energy process.

Table 1. Literature survey of related hybrid electrodes for electrochemical capacitors.

Description	Layered α-$Co(OH)_2$ Nanocones[39]	Co_3O_4/NiO core/shell nanowire arrays[18]	Co-Al hydroxide nanosheets/reduced graphene oxide multilayer films[40]
Specific capacitance	1055 F/g (1 A/g)	2.69 F/cm^2 (6.0 mA/cm^2) 452 F/g (2 A/g)	90 F/m^2 (5 mV/s) 1204 F/g (5 mV/s)
Cycle retention	95% after 2000 cycles (5 A/g)	95.1% after 5000 cycles (6.0 mA/cm^2)	99% after 2000 cycles (20 A/g)
Active Mass loading	0.8-1.6 mg/cm^2	3.0 mg/cm^2	199 ng/cm^2 for one bilayer.
Synthesis method	Solution-based; slurry-pasting	hydrothermal, chemical bath deposition	layer-by-layer assembly

Conclusions

In summary, a simple and flexible solution-based strategy promotes a new interface design for capacitive charge storage, evaporation-induced nickel-cobalt-hydroxide hetero-accumulated nanocrystalline walls on reduced graphene oxide/nickel foams are presented by different Ni-doping and dipping numbers to achieve a balance between a high specific capacitance for the electroactive materials and electrodes with adjustable specific energy and power. It promotes an optimal interface design for the fabrication of high-performance energy conversion and storage devices. However, the interface design still needs an enhanced electron transporting for practical applications with high power and high energy.

Acknowledgements

This work was supported by National Natural Science Foundation of China (21353003), Special Innovation Talents of Harbin Science and Technology (2013RFQXJ145), Fundamental Research Funds of the Central University (HEUCFZ), Key Program of the Natural Science Foundation of Heilongjiang Province (ZD201219), Program of International S&T Cooperation special project (2013DFA50480).

Notes and references

[a] Key Laboratory of Superlight Material and Surface Technology, Harbin Engineering University, Harbin, 150001, China. E-mail: zhqw1888@sohu.com.
[b] Key Laboratory of Cluster Science, Ministry of Education, School of Chemistry, Beijing Institute of Technology, Beijing 100081, China. E-mail: lqu@bit.edu.cn
[c] State Key Laboratory of Polymer Physics and Chemistry, Changchun Institute of Applied Chemistry, Chinese Academy of Sciences, Changchun 130022, China. E-mail: peng.wang@ciac.jl.cn

Electronic Supplementary Information (ESI) available: [details of any supplementary information available should be included here]. See DOI: 10.1039/c000000x/

1 L. Pan, G. Yu, D. Zhai, H. R. Lee, W. Zhao, N. Liu, H. Wang, B. C. K. Tee, Y. Shi, Y. Cui and Z. Bao, *P. Natl. Acad. Sci. USA.*, 2012, **109**, 9287-9292.
2 J. W. Long, B. Dunn, D. R. Rolison and H. S. White, *Chem. Rev.*, 2004, **104**, 4463-4492.
3 A. S. Arico, P. Bruce, B. Scrosati, J. M. Tarascon and W. Van Schalkwijk, *Nat. Mater.*, 2005, **4**, 366-377.
4 M. Pumera, *Energ. Environ. Sci.*, 2011, **4**, 668-674.
5 Q. F. Zhang, E. Uchaker, S. L. Candelaria and G. Z. Cao, *Chem. Soc. Rev.*, 2013, **42**, 3127-3171.
6 S. Xin, Y.G. Guo and L.J. Wan, *Acc. Chem. Res.*, 2012, **45**, 1759-1769.
7 S. Yang, R. E. Bachman, X. Feng and K. Müllen, *Acc. Chem. Res.*, 2012, **46**, 116-128.
8 Q. Lu, J. G. Chen and J. Q. Xiao, *Angew. Chem. Int. Edit.*, 2013, **52**, 1882-1889.
9 W. Wei, X. Cui, W. Chen and D. G. Ivey, *Chem. Soc. Rev.*, 2011, **40**, 1697-1721.
10 P. Yang and J.-M. Tarascon, *Nat. Mater.*, 2012, **11**, 560-563.
11 L. Wang, D. Wang, Z. Dong, F. Zhang and J. Jin, *Nano Lett.*, 2013, **13**, 1711-1716.
12 L.Y. Liang, A. Hirata, T. Fujita and M.W. Chen, *Nat. Nanotechnolo.*, 2011, **6**, 232-236.
13 J. Jiang, Y. Li, J. Liu and X. Huang, *Nanoscale*, 2011, **3**, 45-58.
14 P. Yang, X. Xiao, Y. Li, Y. Ding, P. Qiang, X. Tan, W. Mai, Z. Lin, W. Wu, T. Li, H. Jin, P. Liu, J. Zhou, C. P. Wong and Z. L. Wang, *ACS Nano*, 2013, **7**, 2617-2626.
15 J. Liu, Y. Li, X. Huang, G. Li and Z. Li, *Adv. Funct. Mater.*, 2008, **18**,

1448-1458.
16 G. Q. Zhang and X. W. Lou, *Adv. Mater.*, 2013, **25**, 976-979.
17 J. Liu, J. Jiang, C. Cheng, H. Li, J. Zhang, H. Gong and H. J. Fan, *Adv. Mater.*, 2011, **23**, 2076-2081.
18 X. Xia, J. Tu, Y. Zhang, X. Wang, C. Gu, X.B. Zhao and H. J. Fan, *Acs Nano*, 2012, **6**, 5531-5538.
19 L.Q. Mai, F. Yang, Y.L. Zhao, X. Xu, L. Xu and Y.Z. Luo, *Nat. Commun.*, 2011, **2,**381.
20 H. Cölfen and M. Antonietti, *Angew. Chem. Int. Ed.*, 2005, **44**, 5576-5591.
21 J.W. Liu, H. W. Liang and S.H. Yu, *Chem. Rev.*, 2012, **112**, 4770-4799.
22 W. Chen, S. Li, C. Chen and L. Yan, *Adv. Mater.*, 2011, **23**, 5679-5683.
23 R. B. Rakhi, W. Chen, D. Cha and H. N. Alshareef, *Nano Lett.*, 2012, **12**, 2559-2567.
24 L. Bao and X. Li, *Adv. Mater.*, 2012, **24**, 3246-3252.
25 L. Hu, M. Chen, X. Fang and L. Wu, *Chem. Soc. Rev.*, 2012, **41**, 1350-1362.
26 Y. Ding, M. A. Invernale and G. A. Sotzing, *ACS Appl. Mater. Inter.*, 2010, **2**, 1588-1593.
27 L. Hu, M. Pasta, F. La Mantia, L. Cui, S. Jeong, H. D. Deshazer, J. W. Choi, S. M. Han and Y. Cui, *Nano Lett.*, 2010, **10**, 708-714.
28 Z. L. Wang, D. Xu, J. J. Xu, L. L. Zhang and X. B. Zhang, *Adv. Funct. Mater.*, 2012, **22**, 3699-3705.
29 W. Gao, L. B. Alemany, L. Ci and P. M. Ajayan, *Nat Chem*, 2009, **1**, 403-408.
30 K. Brezesinski, J. Wang, J. Haetge, C. Reitz, S. O. Steinmueller, S. H. Tolbert, B. M. Smarsly, B. Dunn and T. Brezesinski, *J. Am. Chem. Soc.*, 2010, **132**, 6982-6990.
31 T. Brezesinski, J. Wang, S. H. Tolbert and B. Dunn, *Nat. Mater.*, 2010, **9**, 146-151.
32 M. Duduta, B. Ho, V. C. Wood, P. Limthongkul, V. E. Brunini, W. C. Carter and Y. M. Chiang, *Adv. Energ. Mater.*, 2011, **1**, 511-516.
33 J. Liang, R. Ma, N. Iyi, Y. Ebina, K. Takada and T. Sasaki, *Chem. Mater.*, 2010, **22**, 371-378.
34 Z. P. Liu, R. Z. Ma, M. Osada, K. Takada and T. Sasaki, *J. Am. Chem. Soc.*, 2005, **127**, 13869-13874.
35 I. E. Rauda, V. Augustyn, B. Dunn and S. H. Tolbert, *Acc. Chem. Res.*, 2013, **46**, 1113-1124.
36 B. E. Conway, V. Birss and J. Wojtowicz, *J. Power Sources*, 1997, **66**, 1-14.
37 M. Park, X. Zhang, M. Chung, G. B. Less and A. M. Sastry, *J. Power Sources*, 2010, **195**, 7904-7929.
38 D. Wang, R. Kou, D. Choi, Z. Yang, Z. Nie, J. Li, L. V. Saraf, D. Hu, J. Zhang, G. L. Graff, J. Liu, M. A. Pope and I. A. Aksay, *Acs Nano*, 2010, **4**, 1587-1595.
39 L. Wang, Z. H. Dong, Z. G. Wang, F. X. Zhang and J. Jin, *Adv. Funct. Mater.*, 2012, **23**, 2758-2764.
40 X. Y. Dong, L. Wang, D. Wang, C. Li and J. Jin, *Langmuir*, 2012, **28**, 293-298.

Stepwise Interfacial Assemblied Nickel-cobalt-hydroxide Hetero-oriented Nanocrystalline Walls on Reduced graphene oxide/nickel foams: An Adjustable Interface Design for Capacitive Charge storage

Zhongyu Qian, Tao Peng, Liangti Qu, Jun Wang* and Peng Wang*

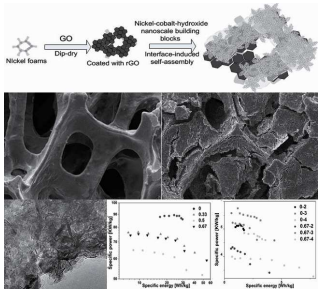

Evaporation-induced nickel-cobalt-hydroxide hetero-accumulated nanocrystalline walls on reduced graphene oxide/nickel foams are presented by different Ni-doping and dipping numbers.